Journal of Zhejiang University-SCIENCE A (Applied Physics & Engineering) in press
www.jzus.zju.edu.cn; www.springer.com/journal/11582
E-mail: jzus_a@zju.edu.cn

Research Article

https://doi.org/10.1631/jzus.A2400540

A dual-focal-plane AR-HUD optical system adapted for heavy-haul locomotives

Huoping YI[1], Fuhao CHANG[1], Yan CHEN[1], Ping TAN[1]✉, Zhen XU[1], Yongbo WU[1], Jin DING[1], Jien MA[2]✉

[1]*College of Automation and Electrical Engineering, Zhejiang University of Science and Technology, Hangzhou 310023, China*
[2]*College of Electrical Engineering, Zhejiang University, Hangzhou 310027, China*

Abstract: Heavy-haul locomotives operate in complex and dynamic environments. Drivers are required to frequently monitor numerous displays within the cab and track conditions, and switching the line of sight will result in driving blind a certain distance. This can easily lead to visual fatigue and safety incidents over extended periods. In this article, we propose a dual-focal-plane augmented reality head-up display (AR-HUD) system adapted for heavy-haul locomotives, integrating dual picture generation units (PGUs) with two freeform surfaces to achieve the display of near-field and far-field. Due to the large inclination angle of the windshield in heavy-haul locomotives, there are significant aberrations of the optical system and the virtual image quality of the far-field needs to be improved. To address this issue, we introduce two freeform surfaces into the optical path of the far-field to reduce aberration. The increased structural degrees of freedom facilitate subsequent optimization. Following optimization of the system, the maximum RMS radius within the eyebox regions E1 to E5 was smaller than the Airy disk radius, and the Modulation Transfer Function (MTF) value at the cutoff frequency exceeded 0.3. Grid distortion was less than 5%, and at the cutoff frequency of 4.31 lp/mm, over 98% of the MTF was greater than 0.3. The image quality and overall imaging performance were excellent, with reasonable tolerance distribution, demonstrating the feasibility of this design. This configuration allows for the simultaneous display of both far-field and near-field images, enhancing its applicability in rail transport. The feasibility of this innovative AR-HUD system has been validated through user interface (UI) simulation.

Key words: Optical system; Off-axis reflective structure; Freeform surface; User interface simulation

1 Introduction

In recent years, the advent of new information technology has facilitated the integration of heavy-haul railways and cutting-edge technology, thereby supporting the construction of intelligent railways. Heavy-haul locomotives operate in complex environments. Drivers must frequently lower their heads or divert their gaze to obtain operational information on the locomotive display, leading to visual fatigue and the risk of overlooking crucial rail condition information. Research has shown that during the entire process of locomotive operation, over 90% of the train driver's gaze time is spent observing visual stimuli such as track conditions and locomotive signals ahead. To obtain information from the instrument panel, an augmented reality head-up display (AR-HUD) system can project essential vehicle information onto the windshield, enabling drivers to access this data without frequently diverting their gaze from the road. This innovation mitigates the risk of accidents associated with frequent shifts in the line of sight. Implementing this technology in heavy-haul traffic not only alleviates a driver's visual fatigue but also aligns with the 14th Five-Year Plan for Railway Science and Technology Innovation in China.

The field of AR-HUD technology has witnessed a period of rapid development in recent years. A variety of research has been conducted on the development and design of AR-HUDs. Wang et al. (2024) studied the impact of dynamic distortion in

✉ Ping TAN, 115011@zust.edu.cn
Jien MA, majien@zju.edu.cn
Huoping YI, https://orcid.org/0009-0007-4615-6528
Ping TAN, https://orcid.org/0000-0001-8656-3514

Received Nov. 27, 2024; Revision accepted Dec. 24, 2024; Crosschecked

automotive HUDs. Through carefully designed experimental scenarios, this research evaluated the subjective experience of drivers at different levels of distortion, providing valuable guidance for optimizing HUD systems. Wang et al. (2023) reviewed the research progress on vergence-accommodation conflict (VAC) in enhanced near-eye displays. They analyzed in detail the causes of VAC and potential solutions, including multi-focal-plane, light field display, and variable parallax technology. The article provides research directions and technical references for improving the visual experience of AR near-eye displays. Ran et al. (2022) proposed a method of using ray tracing to solve the minimum diffuse circle position and determine the three-dimensional coordinates of HUD virtual image points within the eye movement range, providing a new technical means for evaluating the quality and optimizing the design of HUD system virtual images.

Huang et al. (2019) applied digital light processing (DLP) technology to projection and designed an optical path projection system with a virtual image viewing distance of 7.5 m and a field of view (FOV) of 9.8° by 5.5°. However, traditional AR-HUDs are usually fixed-focus structures, which cause conflicts between eye vergence and accommodation and result in visual discomfort during extended periods of driving. To mitigate these issues, it is feasible to design optical systems with multiple projected virtual images or optical systems with variable projection distances. Sun et al. (2024) designed an HUD system featuring a variable projection distance of 3-10 m, a virtual image FOV of 15° by 5°, and an eyebox size of 130 by 50 mm. However, the system lacks segmentation of the virtual image, which can result in visual interference. Furthermore, the adjustment of projection distance is achieved through mechanical movement, requiring regular maintenance of the mechanical components. In consideration of the typical visual demands of driving, an optimal optical structure should use multiple virtual images at various depths to effectively display different types of information. Liu et al. (2023) proposed a dual-focal-plane AR-HUD using polarization multiplexing, wherein each virtual image leverages the full resolution of a picture generation unit (PGU). While this enhances imaging quality, it is essential to consider the operational lifespan of the motors for practical applications to ensure the continuity of imaging.

Dual-focal-plane AR-HUDs have been studied by Kong and Xue (2022), who developed a dual-focal-plane AR-HUD system with virtual image distances (VIDs) of 2.5 m and 7.5 m, using dual PGUs. By segmenting the virtual image content into distinct regions, the system ensures high imaging quality. Nonetheless, this approach results in a large overall size. Jiang and Guo (2023) engineered a dual-focal vehicle coupled adjustable AR-HUD system, which can display navigation information at any distance from 8 to 24 m through the axial movement of three folding surfaces. This extensive adjustment range in the far field optical path enhances the augmented reality performance. The principle is that the greater the object distance, the greater the VID. The virtual image will also be larger without changing the size of the PGU image. However, this structure is costly and its practicality needs further improvement. Furthermore, AR-HUD optical systems can adjust the FOV through holography and diffraction techniques, adjust the depth distance of virtual images, and design the optical structure of multiple virtual images. These methods aim mainly to advance augmented reality exploration. However, due to current technological limitations and cost considerations, they have not yet progressed to the stage of mass production.

In this article we present a feasibility analysis of AR-HUD technology in the heavy-haul locomotive sector, drawing on practical experience from collaboration with the Shuozhou-Huanghua Railway Group. A dual-focal-plane AR-HUD system has been designed for rail transportation. The system uses two freeform surfaces to reduce aberrations, thereby enhancing the clarity of the far-field virtual image. Following optimization, the maximum RMS radius within the eyebox regions E1 to E5 is smaller than the Airy disk radius, and the Modulation Transfer Function (MTF) value at the cutoff frequency exceeds 0.3. Grid distortion is less than 5%, and at the cutoff frequency of 4.31 lp/mm, over 98% of the MTF is greater than 0.3. The image quality, user interface (UI) simulation, and overall imaging performance are excellent, with reasonable tolerance distribution, demonstrating the feasibility of this design. The system displays basic locomotive information and

interactive information on separate screens, ensuring they do not interfere with each other. This separation mitigates the VAC, reducing visual fatigue for drivers and enhancing safety.

2 Principles of optical structure design

2.1 Principle of the dual-focal-plane AR-HUD optical system

The imaging of HUD is based on the principles of optical reflection and projection imaging. Fig. 1 illustrates the classical structure of an HUD. It comprises two freeform surfaces, a PGU, and a windshield. The overall optical structure is processed off-axis, with freeform surfaces offering greater flexibility compared to conventional surfaces, and which can be optimized to the maximum extent for the actual use of space. Light is emitted from the PGU, successively reflected and refracted by the freeform surfaces 1 and 2, ultimately reaching the windshield and entering the human eye. The driver's brain emits a signal that light propagates in straight lines, which are then traced back through the eyes and projected onto the windshield.

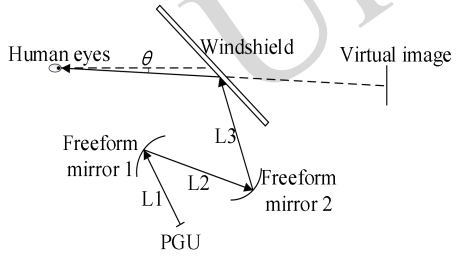

Fig. 1 Schematic diagram of the classical structure of an HUD optical system

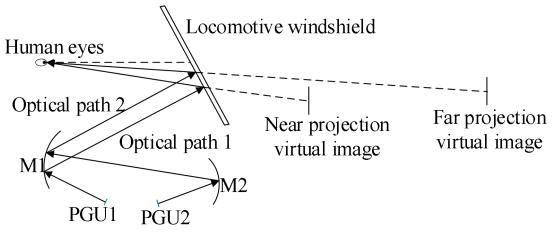

Fig. 2 Schematic diagram of the dual-focal-plane AR-HUD optical structure

In consideration of the available space under the locomotive operator console, we selected a coaxial three-reflector optical system as the starting point. It then carries out off-axis processing to optimize the design of the off-axis three-reflector optical system, which can design the optical structure more compactly. The locomotive windshield surface is of the irregular surface type. The optical reflector in the off-axis three-reflector structure can correct aberration. The optical structure described here consists of the near optical path and the far optical path, and contains two PGUs and two freeform surfaces. The use of a single PGU to display the far-field and near-field images results in a reduction in the resolution of the virtual image. Therefore, we use two PGUs in the design, with the space under the heavy-haul locomotive operator console meeting the requisite volume requirements.

Fig. 2 illustrates the internal structure of the dual-focal-plane AR-HUD. The near optical path begins with PGU1, which reflects directly to the freeform surface M1. The light is then reflected onto the windshield and into the human eye. Due to the large inclination angle of the windshield in heavy-haul locomotives, the designed optical structure differs somewhat from that applied to automobiles.

The optical structure for a heavy-haul locomotive (Fig. 2) is more challenging to design. The windshield inclination angle of the "Shenhua" heavy-haul locomotive is about 65°, significantly steeper than the 45° inclination angle typical of automobile windshields. In the HUD optical design for heavy-haul locomotives, this pronounced inclination introduces greater optical aberrations compared to those encountered in standard automotive HUD systems. This makes it challenging to achieve aberration correction far-field using a single freeform reflective surface. Therefore, based on sharing M1 between far-field and near-field, a freeform surface M2 was introduced to improve design flexibility. The incorporation of two freeform reflective surfaces not only facilitates the optimization of image quality but also provides the potential to further reduce the optical system's volume while maintaining imaging performance. In the far optical path, light from PGU2 first reflects off M2, then off M1, and finally onto the windshield and into the driver's eye. The light is then back-traced and projected onto the region in front of the windshield. The far optical path projects the guidance information of the locomotive, and the dual freeform surfaces

effectively corrects the aberration of the windshield surface to obtain a clearer image. This dual-focal-plane AR-HUD optical structure design has a wide range of applicability, here exemplified by a "Shenhua" model from the Shuozhou-Huanghua Railway Group, which has been successfully implemented in this locomotive model.

2.2 Fitting of freeform surfaces

The windshield of heavy-haul locomotives has complex non-planar characteristics. Light passing through it introduces optical distortions such as aberrations and non-uniform refraction, which affects the quality of the projected image. Furthermore, the windshield of heavy-haul locomotives has a steeper inclination angle than automobile windshields, resulting in even greater aberrations in the optical system.

To address these challenges, freeform surfaces are required for precise fitting. Zernike freeform surfaces can flexibly adjust the surface shape and are suitable for systems that work with complex curved glass. Moreover, Zernike freeform surfaces are closely related to Seidel aberrations, enabling the correction of distortions caused by irregular windshield surfaces. This significantly enhances the imaging performance of optical HUD systems. The Zernike polynomial freeform surface is defined by the sag equation:

$$Z(x,y)=\frac{cr^2}{1+\sqrt{1-(1+k)c^2r^2}}+\sum_{i=1}^{M}a_i r^{2i}+\sum_{i=1}^{N}A_i E_i(x,y), \tag{1}$$

where c denotes the surface curvature, k denotes the conic coefficient, A_i is the coefficient of the first Zernike standard polynomial, a_i signifies the aspheric coefficient, r indicates the radial length, and N corresponds to the ordinate of the Zernike coefficient. The extension and parameter relationship of the Zernike polynomial equation can be derived from Eq. (S1) and Eq. (S2) in the electronic supplementary materials (ESM).

3 Design parameters

The main parameters of the optical system designed in this programme are eyebox dimensions, VID, FOV, and PGU.

The eyebox indicates the region where the display content is clearest. According to the average distance of the human eye, the designed eyebox dimensions are 130 by 50 mm. Considering that the maximum speed of a heavy-haul locomotive does not exceed 120 km/h, the overall operating speed is relatively slow. A far-field distance set to 10 m, and a near-field distance set to 3 m meets the requirements.

The usage scenarios vary substantially from those of automotive HUDs, when designing the FOV for the optical system, consideration must be given to the operational environment of heavy-haul locomotives. Due to the prolonged operating periods and the complexity of the environments in which these locomotives operate, it is necessary to redefine the FOV based on the following perspectives.

First, when navigating challenging terrains such as uphill and downhill slopes, tunnels, and curves, drivers must manage the locomotive's traction and speed while simultaneously monitoring critical information in real time, such as slope gradients, tunnel lengths, and upcoming curves. Additionally, drivers are tasked with visually assessing the track conditions, identifying signal lights, and detecting potential obstacles. Safety considerations are predominantly focused within the track region, as most operational decisions hinge on information from this zone. Given this, the track region becomes the logical projection region for the AR-HUD system.

For standard rail tracks in China, which have a width of 1435 mm, the optimal FOV for the AR-HUD remote projection screen is initially set to 8° by 4°. However, to accommodate the driver's need for broader situational awareness, particularly on both sides of the track, the FOV is expanded to 10° by 4° to ensure comprehensive coverage.

The virtual image sizes, PGU dimensions, and resolutions can be derived from the VIDs and FOVs. Based on the known values of the VID and FOV in optical systems, the virtual image sizes (calculated by Eq. (S3) and Eq. (S4) in the ESM) for distances of 10 m and 3 m are 1749.77 mm by 698.42 mm and 209.52 mm by 52.36 mm, respectively.

The human eye can distinguish objects with a visual angle limit of 1', equivalent to 1/60°. Under normal conditions, the pixel size of the PGU must

exceed this value. Otherwise, individual pixels cannot be resolved. Using Eq. (2), the resolvable pixel sizes for VIDs of 10 m and 3 m are calculated to be 2.91 mm and 0.87 mm, respectively.

$$\mu = V \times \tan(1/60°), \tag{2}$$

$$\lambda = \frac{1}{2 \times p}. \tag{3}$$

Where μ is the pixel size, V is the VID. Then, based on the known virtual image size, the smallest pixel that can be resolved by the human eye in the horizontal direction is 905 pixels. This value is used to limit the resolution of the PGU in the horizontal direction in our optical design. Given that we are adopting a dual PGU scheme and considering the strong light exposure in the heavy train operating environment, it is crucial to enhance the brightness of the virtual image and address the potential issue of sunlight backflow. Consequently, we have selected DLP technology for the PGU. DLP technology not only solves the problem of sunlight backflow but also achieves higher source image brightness. Following design optimization, the effective source image sizes are 153.6 mm by 64.08 mm for far-field and 79.62 mm by 23.16 mm for near-field, with resolutions of 1280 by 640 and 680 by 200 pixels, respectively. Using Eq. (3), we can determine the limiting resolution of the optical system.

The parameter λ is the limiting resolution of the optical system, while p denotes the pixel size. For both 10 m and 3 m optical paths, the maximum spatial frequency is about 4.31 line pairs per millimeter (lp/mm). To ensure optimal image quality, the MTF value for both the far and near optical paths must exceed 0.3 at 4.31 lp/mm. Additionally, the distortion rate should be maintained below 5%. Finally, the design specifications of the AR-HUD optical system adapted for heavy-haul locomotives are shown in Table 1.

Table 1 Design parameters of the optical system

HUD system parameters	Parameter Value
VID /m	Near: 3 Far: 10
FOV /(°)	Near: 4° by 1° Far: 10° by 4°
Eyebox /mm	130 by 50
Pupil diameter /mm	5
Wavelength /μm	0.55
PGU	DLP: 680 by 200 DLP: 1280 by 640
Distortion /%	<5
MTF /(lp/mm)	Center: >0.5@4.31 Other: >0.3@4.31

4 Design of the optical system and optimization results

4.1 Optical design process

In designing the dual-focal-plane AR-HUD system, it was first necessary to obtain the surface data of the locomotive windshield. The optimal method involves fitting the engineering file of the windshield and then inserting the fitted data into the sequence pattern for system design optimization. To maximize practical application fit, the windshield data in this study were provided by the Shuozhou-Huanghua Railway. The Zernike standard sag surface type expression was used, exhibiting a radius of curvature of −2426 mm and a normalized radius of 100 mm, with 15 Zernike coefficients set at 0, 8.401×10^{3}, −12.310, 2.035×10^{-9}, 4.740×10^{-9}, -3.133×10^{-7}, 4.073×10^{-9}, -2.901×10^{-7}, 2.919×10^{-9}, 2.826×10^{-9}, -9.659×10^{-9}, -2.839×10^{-6}, -2.477×10^{-5}, -5.466×10^{-4}, and 6.2656×10^{3}.

In the optical path design process, the system was initially constructed as a coaxial optical path, then was achieved off-axis by rotating and decentering the freeform surface. Next, we added boundary conditions, such as image size, aperture, center FOV position, lens center position, angle of incident light on the image surface, imaging size, and aberration constraints using the merit function editor. Freeform surfaces and PGUs were positioned appropriately to avoid component overlap and light masking. During optimization, by constraining the boundary conditions and evaluation indicators and controlling the curvature, thickness, rotation, and decentering of the freeform surface along with the parameters of the surface fit, the evaluation indicators were initially set at an average level and gradually increased until they reached the optimal imaging state.

The diaphragm surface was defined in the center of the window, and the pupil of the human eye was used as the system diaphragm. The pupil of the human eye normally ranges from 2-5 mm. To ensure that all the light could enter the eye, we set the diameter of the pupil at 5 mm. To simulate the visual effect of the

eye in different regions of the eyebox, we set five coordinate points in the eyebox: the upper left, upper right, middle, lower left, and lower right. Each of these coordinate points included nine FOVs. The movement of the human eye at these five coordinate points was achieved through multiple structures. The two VIDs were 10 m and 3 m, respectively, with corresponding FOVs of 10° by 4° and 4° by 1°. Additionally, a 1° interval between the near and far FOV was used to prevent the near-field image from blocking the far-field light path. Fig. 3 is a schematic diagram of the distribution of the optical pupil in the eyebox. Fig. 4 is a schematic diagram of the FOV setup. A 3D schematic diagram of the optimized optical path is shown in Fig. 5. Figs. 6a and 6b show a detailed schematic diagram of the optimized optical path.

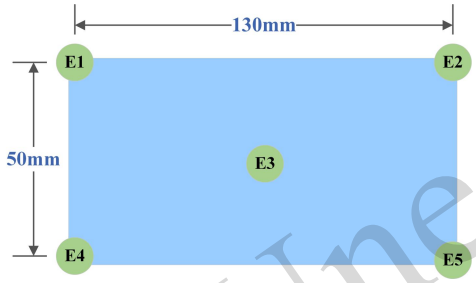

Fig. 3 Schematic diagram of pupil distribution in the eye box

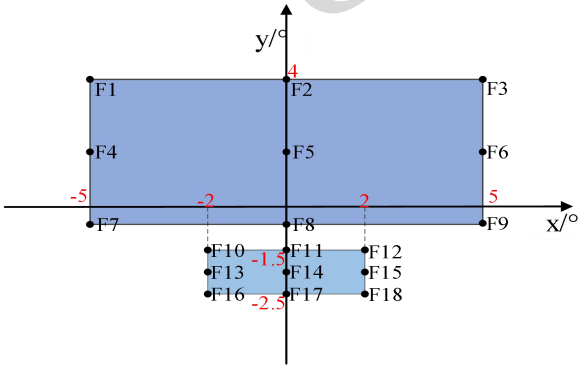

Fig. 4 Schematic diagram of the FOV settings

Fig. 5 Schematic diagram of the dual-focal-plane AR-HUD system structure

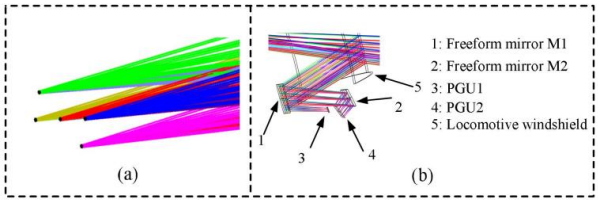

Fig. 6 (a) Structural diagram of eyebox regions E1~E5; (b) Schematic diagram of the internal structure of the dual-focal-plane AR-HUD system

4.2 Image quality evaluation

Upon completing the optimization, it was essential to analyze the image quality of both the far-field and near-field. We used spot diagrams, MTF curves, and grid distortion diagrams to evaluate the virtual image quality. Figs. 7a and 7b show the spot diagrams for the far-field and near-field across the five specified regions within the eyebox (E1 to E5). Fig. 7 shows that the results for each FOV within the eyebox regions fell within the Airy disk. The maximum RMS radius was 56.25 μm, which is below the empirical design threshold of 80 μm for AR-HUD systems, thereby confirming that the image quality met the required standards.

The MTF curves are illustrated in Figs. 8a and 8b. The pixel size of the PGU was about 0.116 mm, with the maximum spatial frequency of the system around 4.31 lp/mm. At a projection distance of 10 m, the MTF values within the eyebox regions E1 to E5 exceeded 0.3 at 4.31 lp/mm. Similarly, at a projection distance of 3 m, the MTF values also surpassed 0.3. These results indicate that the optical system met the required image quality standards.

Fig. 9 illustrates the grid distortion diagrams. Fig. 9a shows the grid distortion at the center FOV for a projection distance of 10 m, with the maximum edge distortion at 3.1127%, indicating no noticeable deformation during viewing. Fig. 9b illustrates the grid distortion at the center FOV for a projection distance of 3 m, with the maximum edge distortion at 1.2071%. Both optical paths exhibit maximum distortions of less than 5%, thereby meeting the design specifications of the optical system.

Fig. 10 illustrates the locomotive far-field display interface, which was designed using Qt software.

Fig. 10a depicts the original image of the far-field, which was simulated by the optical system. Fig. 10b

shows the UI simulation effect of the center FOV at a projection distance of 10 m. Fig. 11 shows the locomotive near-field display interface, which was designed with Qt software. Fig. 11a depicts the original image of the near-field, which was simulated by the optical system. Fig. 11b shows the UI simulation effect of the center FOV at a projection distance of

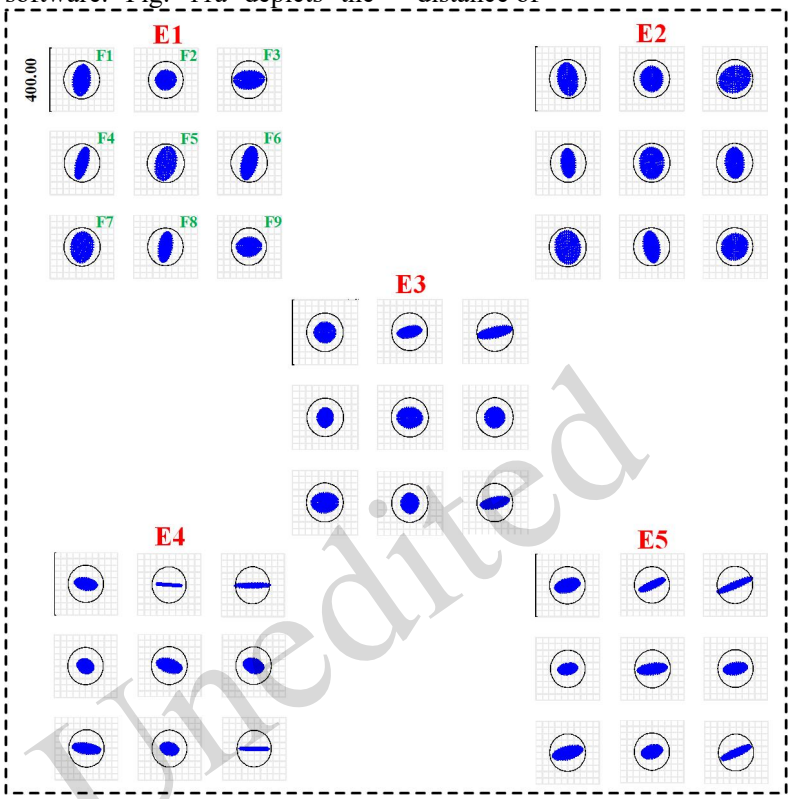

(a)

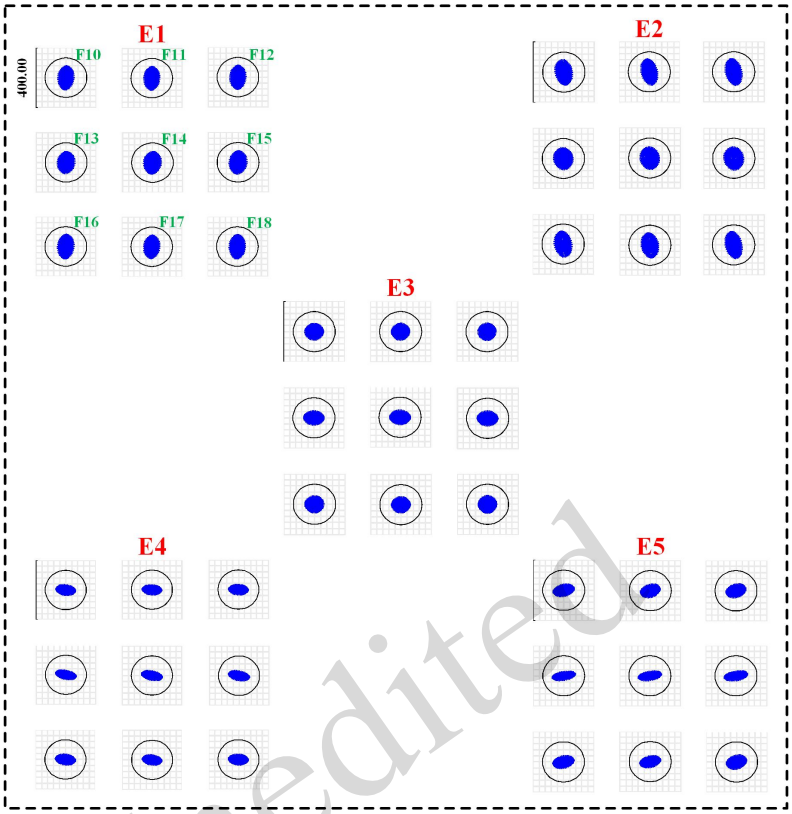

(b)

Fig. 7 (a) Spot diagrams of eyebox regions E1~E5 with a projection distance of 10 m; (b) Spot diagrams of eyebox regions E1~E5 with a projection distance of 3 m

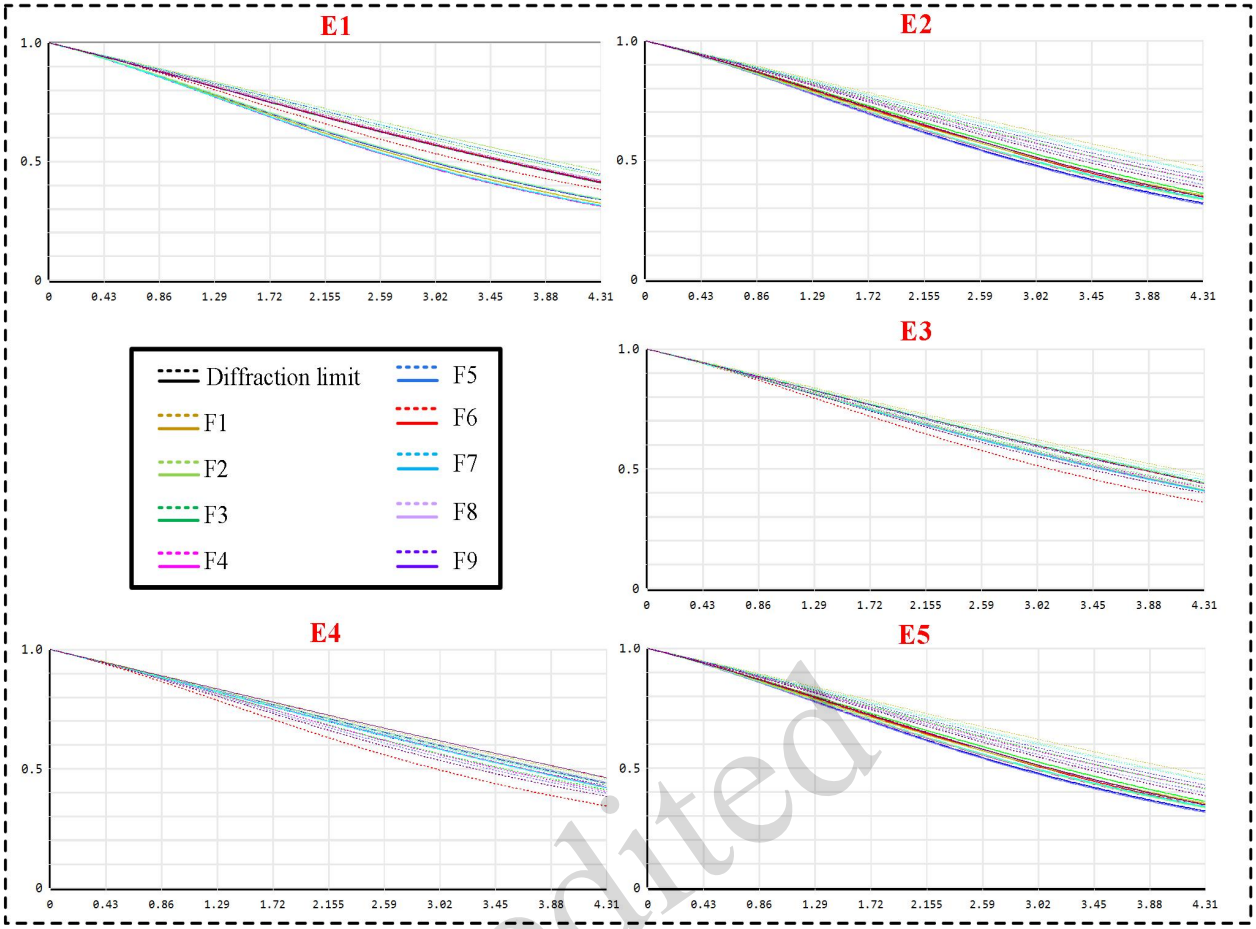

(a)

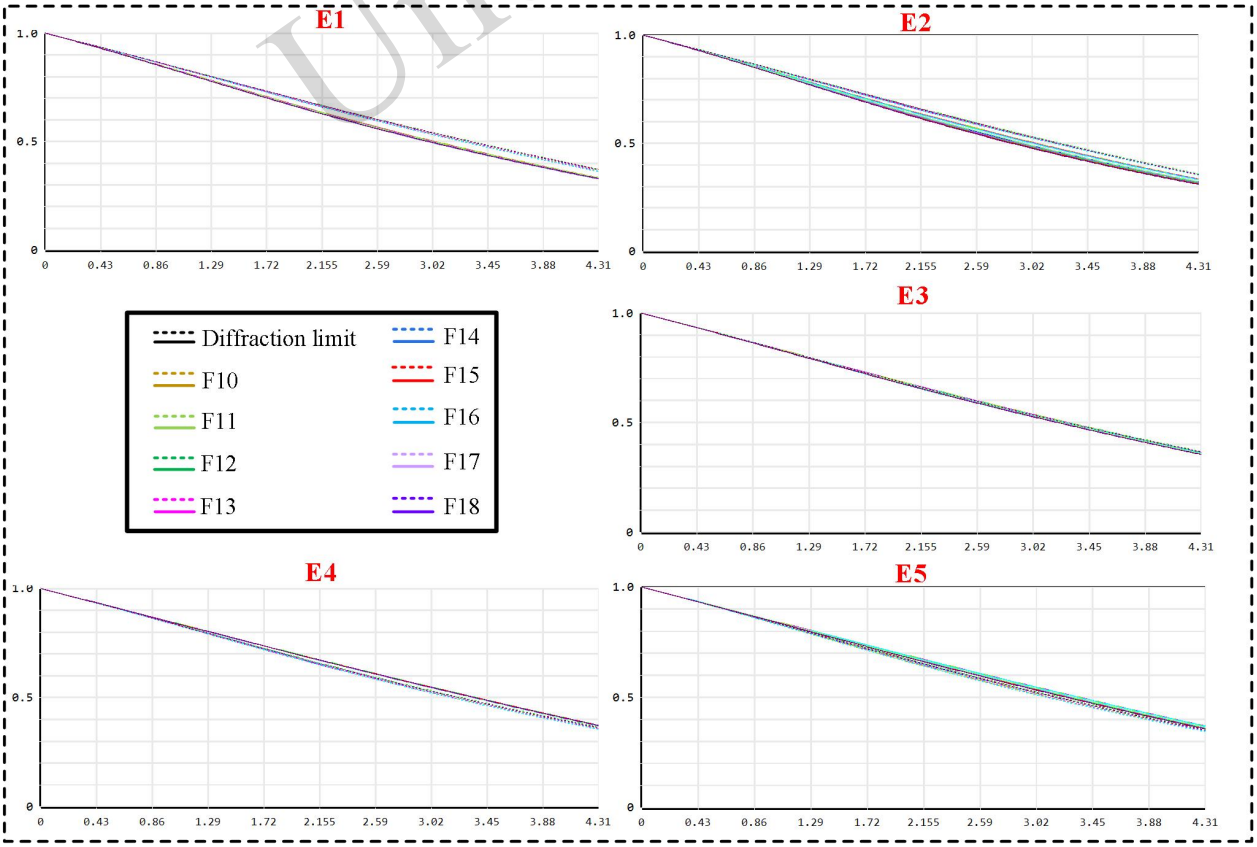

(b)

Fig. 8 (a) MTF curve of the eyebox regions E1~E5 at a projection distance of 10 m; (b) MTF curve of the eyebox regions E1~E5 at a projection distance of 3 m

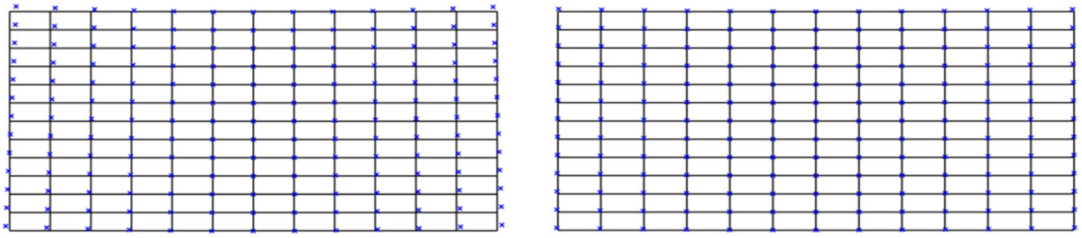

Fig. 9 (a) Mesh distortion diagram at a projection distance of 10 m; (b) Mesh distortion diagram at a projection distance of 3 m

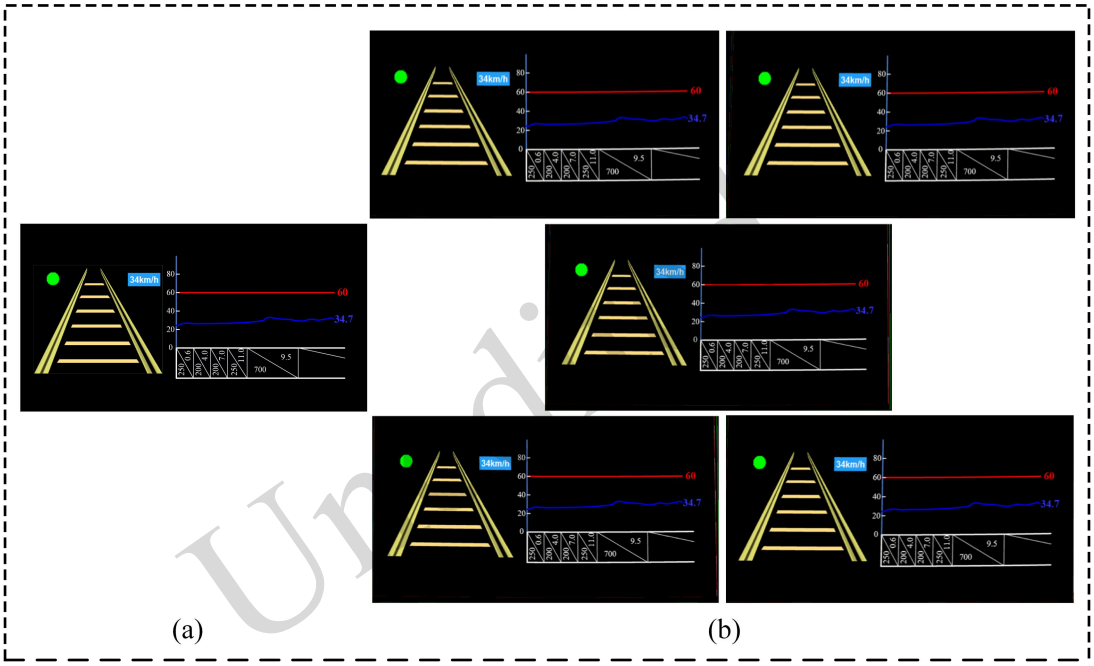

Fig. 10 (a) Far-field original image used for simulation; (b) UI simulation rendering of eyebox regions E1~E5 with a projection distance of 10 m

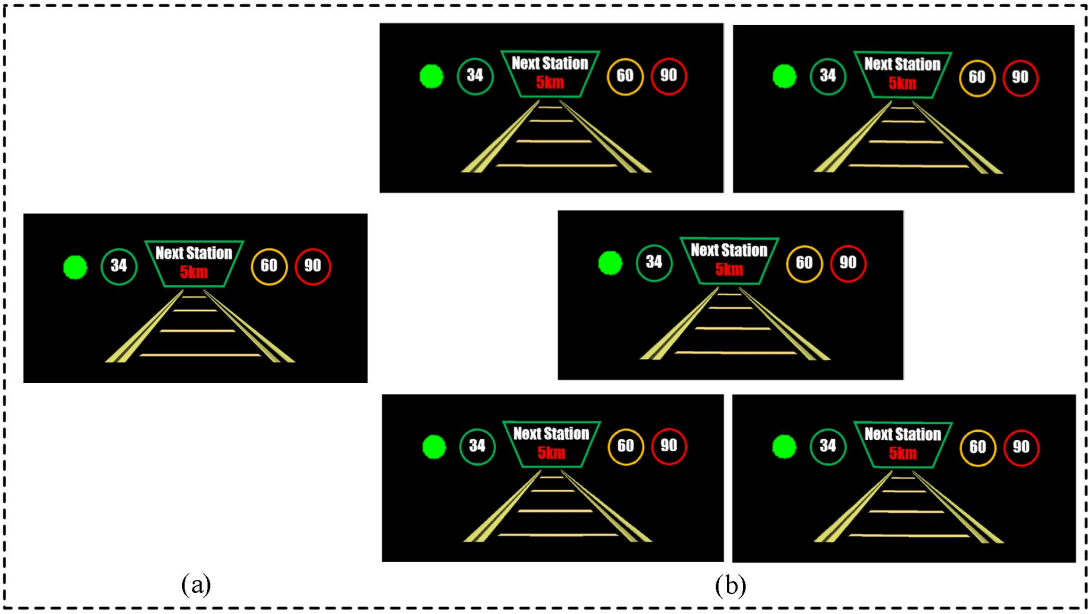

Fig. 11 (a) Near-field original image used for simulation; (b) UI simulation rendering of eyebox regions E1~E5 with a projection distance of 3 m

3 m. The far-field and near-field virtual image surfaces can be observed intuitively. A comparison between the final simulated image and the original image reveals that the UI simulation image of the dual-focal-plane optical system exhibits a superior imaging effect.

Dynamic distortion describes the variation in image shape and position perceived when the line of sight shifts from the center to other regions within the eyebox. The distortion in moving images at various positions within the eyebox can be evaluated using the calculation method presented in Eq. (4),

$$E = 60 \times \arctan(|(x_{ij}, y_{ij}) - (x_{1j}, y_{1j})| \div L). \quad (4)$$

Where i denotes the four edge points of the eyebox, j represents the nine FOV points within the eyebox, and L stands for the virtual image distance. The primary objective was to calculate the distance between the FOV coordinates of the four edge points of the eyebox and the FOV coordinates at the central point, followed by calculating the angular displacement of this distance relative to the human eye. The actual coordinates of each FOV point within the eyebox can be obtained through ray tracing. The final calculation results are presented in Tables 2 and 3. Configuration 1 corresponds to the center of the eyebox, while configurations 2 to 5 represent the four edge points of the eyebox: upper left, upper right, lower left, and lower right, respectively. P1-P9 represent the nine FOVs of a certain point in the eyebox. Table 2 shows the dynamic distortion results for the far-field, and Table 3 presents the results for the near-field. The maximum value of dynamic distortion was less than 5', indicating that the variation in dynamic distortion meets empirical standards and has minimal impact on the human eye's normal observation of the image.

Binocular disparity is a critical parameter in HUD design. For our dual-focal-plane optical system, we tested vertical binocular disparity. When viewed through binocular lenses, the two eyes often have a slight angular disparity when focusing on the same point in the image. In an ideal system, this angle is zero. However, in practical HUD design, this disparity angle should be within 2.5 mrad. Exceeding this threshold can cause discomfort and visual fatigue. With an average interpupillary distance of 65 mm, to

Table 2 Dynamic distortion results for the far-field

Position	Config2-1	Config3-1	Config4-1	Config5-1
P1	0.61	0.55	0.58	0.62
P2	0.60	0.57	0.64	0.71
P3	0.83	0.86	0.90	1.01
P4	0.44	0.47	0.40	0.45
P5	0.68	0.65	0.68	0.73
P6	0.55	0.55	0.53	0.57
P7	0.72	0.67	0.73	0.78
P8	0.51	0.46	0.47	0.50
P9	0.71	0.70	0.75	0.84

Table 3 Dynamic distortion results for the near-field

Position	Config2-1	Config3-1	Config4-1	Config5-1
P1	1.66	1.74	1.72	1.82
P2	1.58	1.68	1.70	1.73
P3	1.61	1.70	1.73	1.76
P4	1.75	1.87	1.79	1.98
P5	1.78	1.90	1.82	2.00
P6	1.81	1.93	1.85	2.04
P7	1.69	1.78	1.76	1.86
P8	1.63	1.71	1.69	1.80
P9	1.65	1.74	1.76	1.79

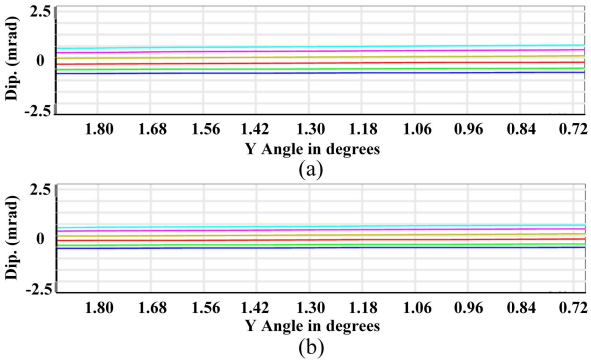

Fig. 12 Simulation results of binocular disparity for far-field in the regions of the eyebox. (a) E1 and E2; (b) E4 and E5

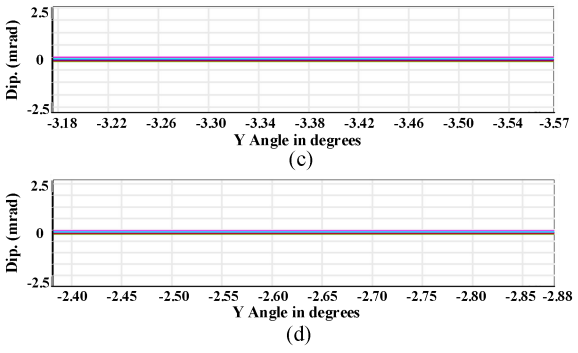

Fig. 13 Simulation results of binocular disparity for near-field in the regions of the eyebox. (a) E1 and E2; (b) E4 and E5

simulate the worst-case scenario, we evaluated the binocular disparity at the left and right edges of the eyebox. The simulation results of binocular disparity, with both eyes positioned at the edges of the eyebox, are shown in Fig. 12 and Fig. 13. The final results imply that the designed binocular disparity of the optical system for both far-field and near-field meets the specified range and remains well below the target value.

4.3 Tolerance analysis

Tolerance analysis is a crucial step in optical design. Its main purpose is to limit the machinable error range and appropriately reduce manufacturing and processing costs without affecting the imaging quality of the optical system. The tolerance parameters should be constrained within an appropriate range. If they are too small, processing and assembling optical components will become more difficult, and costs will increase. If they are too large, it will affect the imaging quality.

Table 4 shows the range of tolerance allocation. Through tolerance analysis using ZEMAX software, 1000 Monte Carlo samples were selected, and the statistical results of the optical transfer function are shown in Table 5. At the cutoff frequency of 4.31 lp/mm, over 98% of the MTF was larger than 0.3. This suggests that the tolerance allocation is suitable and that the optical structure meets the expected requirements.

Table 4 System tolerance allocation

Tolerance parameters	The radius of curvature /mm	Spacing /mm	X/Y direction offset /mm	The amount of rotation on the X/Y axis /(°)
Windshield	1	0.2	0.2	0.2
First mirror	1	0.2	0.2	0.2
Secondary mirror	1	0.2	0.2	0.2

Table 5 Results of monte carlo analysis

Percentage /%	MTF at a projection distance of 10 m	MTF at a projection distance of 3 m
98	0.35487903	0.65880923
90	0.35498960	0.65893926
80	0.35504303	0.65901983
50	0.35515077	0.65916228
20	0.35526619	0.65927341
10	0.35532294	0.65933422
2	0.35542353	0.65939313

4.4 Experimental verification

To validate the effectiveness of our design, we conducted an AR-HUD practical effect experiment following the successful achievement of all simulation results. The fabrication process of the prototype largely mirrored that of a conventional AR-HUD prototype. The freeform reflective surface was meticulously machined using a diamond turning machine. Subsequently, a protective aluminum film was applied to the reflective surface to prevent oxidation, thereby preserving the imaging quality. The mechanical housing was partially realized through 3D printing technology. Finally, the precisely machined primary mirror, secondary mirror, and PGU were assembled in their predetermined positions. Fig. 14 shows the completed AR-HUD prototype, while Fig. 15 shows the heavy-haul locomotive windshield experiment platform.

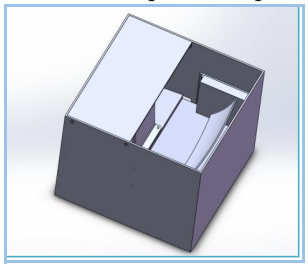

Fig. 14 Diagram of the AR-HUD prototype

Fig. 15 Diagram of the windshield experiment platform

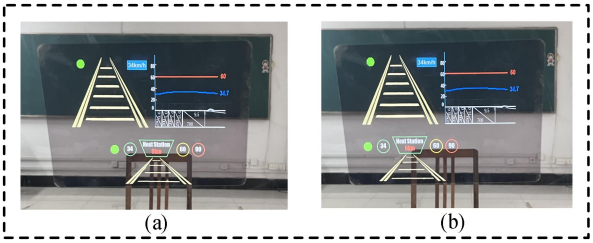

Fig. 16 (a) Virtual images of far-field and near-field at the center of the eyebox; (b) Virtual images of the far-field and near-field when the center of the eyebox is moved horizontally to the edge

To verify the VID of the two FOVs, a blackboard and chair were placed at distances of 10 m and 3 m in front of the windshield, respectively. A camera was then used to capture the virtual image. Fig. 16a shows the virtual image captured at the center of the eyebox, while Fig. 16b illustrates the virtual image when the center of the eyebox was shifted horizontally to the edge. The positional relationship between the far-field virtual image and blackboard at 10 m remains almost unchanged. In contrast to the preceding, the relationship between the near-field virtual image and chair at 3 m shows a significant alteration. This indicates that the far-field virtual image and blackboard at 10 m are located at the same depth. Similarly, the near-field virtual image and chair at 3 m are situated at the same depth.

5 Conclusions

In this paper, we present the design of a dual-focal-plane AR-HUD optical system, based on the driving environment of locomotive drivers. The main purpose is to reduce driver fatigue and enhance the safety of heavy-haul locomotive operation through optical design. The design results were analyzed in terms of image quality and tolerance. The results of the analyses showed that the maximum RMS radius within the eyebox regions E1 to E5 was smaller than the Airy disk radius. Furthermore, the MTF value at the cutoff frequency was greater than 0.3, and the grid aberration was less than 5%. At the cutoff frequency of 4.31 lp/mm, over 98% of the MTF was greater than 0.3, indicating good imaging quality and reasonable tolerance allocation, thus proving the feasibility of this design. This approach uses two light sources to separately display the interaction information between the locomotive and the road, as well as the basic information of the locomotive itself, thereby reducing safety hazards during operation. Additionally, the far optical path corrects aberrations through two Zernike surfaces, improving the imaging quality of the far-field. Future advancements could include the incorporation of software algorithms to detect whether the virtual image plane is focused and the addition of hardware circuits to fine-tune PGU2, to ensure the virtual image plane always remains in focus. This would further enhance the imaging effect and stability of the virtual image plane.

Acknowledgments

This study was supported by the Key R&D Plan Projects in Zhejiang Province (2023C01243), China and The National Natural Science Foundation of China (Nos. 52472422, 52293424, 52477065).

Author contributions

Huoping YI designed the research. Fuhao CHANG wrote the first draft of the manuscript. Yan CHEN and Ping TAN processed the corresponding data. Zhen XU and Yongbo WU helped to organize the manuscript. Jing DING and Jien MA revised and edited the final version.

Conflict of interest

Huoping YI, Fuhao CHANG, Yan CHEN, Ping TAN, Zhen XU, Yongbo WU, Jing DING, and Jien MA declare that they have no conflict of interest.

References

An Z, Meng XP, Ji X, et al., 2021. Design and Performance of an Off-Axis Free-Form Mirror for a Rear Mounted Augmented-Reality Head-Up Display System. *IEEE Photonics Journal*, 13(1):1-15. https://doi.org/10.1109/JPHOT.2021.3052726

Dai GY, Han Y, Yi LQ, et al., 2024. Compact pupil-expansion AR-HUD based on surface-relief grating. *Optics Express*, 32(5):6917-6928. https://doi.org/10.1364/OE.513577

Ding Y, Zhang NW, Yang C, et al., 2024. Design of freeform low-distortion automotive lens based on point-by-point construction. *Acta Optica Sinica*, https://link.cnki.net/urlid/31.1252.O4.20240424.1034.006

Fan RD, Wei SL, Ji HR, et al., 2023. Automated design of freeform imaging systems for automotive heads-up display applications. *Optics Express*, 31(06):10758-110774. https://doi.org/10.1364/OE.484777

Fan CX, Kong LB, Yang B, 2023. Design of Dual-Focal-Plane AR-HUD Optical System Based on a Single Picture Generation Unit and Two Freeform Mirrors. *Photonics*, 10(11):1192. https://doi.org/10.3390/photonics10111192

Huang XZ, Hu SJ, Tang GM, et al., 2019. Optical Structure Design of Automobile Head-up Display with Long-distance Imaging. *Journal of Applied Optics*, 40(5):897-900. https://doi.org/10.57-68/JAO201940.0505006

Jiang QB, Guo ZY, 2023. AR-HUD Optical System Design and Its Multiple Configurations Analysis. *Photonics*, 9:954. https://doi.org/10.3390/photonics10090954

Kong XX, Xue C, 2022. Optical Design of Dual-Focal-Plane

Head-Up Display Based on Dual Picture Generation Units. *Acta Optica Sinica*, 42(14):188-193. https://doi.org/10.3788/AOS202242.1422003

Liu Y, Dong JQ, Qiu YQ, et al., 2023. Compact dual-focal augmented reality head-up display using a single picture generation unit with polarization multiplexing. *Optics Express*, 31(22):35922-35936. https://doi.org/10.1364/OE.502617

Lv ZL, Liu J, Yang Y, et al., 2022. Dual-View and Multi-Content Head-Up Display Using a Single Picture Generation Unit and Two-Layer Volume Holographic Grating. *IEEE Photonics Journal*, 14(4):1-8. https://doi.org/10.1109/JPHOT.2022.3181620

Lv ZL, Liu J, Xu LF, et al., 2021. A Multi-Plane Augmented Reality Head-Up Display System Based on Volume Holographic Optical Elements with Large Area. *IEEE Photonics Journal*, 13(5):1-8. https://doi.org/10.1109/JPHOT.2021.3105670

Li Y, Li Y, He YL, et al., 2018. Design of compact freeform off-axis three-mirror system. *Journal of Applied Optics*, 39(6):780-784. https://doi.org/10.5768/JAO2018-39.0601003

Merenda C, Kim H, Tanous K, et al., 2018. Augmented Reality Interface Design Approaches for Goal-directed and Stimulus-driven Driving Tasks. *IEEE Transactions on Visualization and Computer Graphics*, 24(11):2875-2885. https://doi.org/10.1109/TVCG.2018.2868531

Pan Y, Liu H, Liu HJ, et al., 2021. Feasibility analysis of head-up display technology applied to railway transportation. *Control and Information Technology*, 6:91-95. https://doi.org/10.13889/j.issn.2096-5427.2021.06.013

Pan GY, 2018. Prospects of the application of head-up display system in high-speed rolling stock industry. *Railway Locomotive and Motor Car*, 12:47-48.

Qin Z, Lin SM, Luo KC, et al., 2019. Dual-focal-plane augmented reality head-up display using a single picture generation unit and a single freeform mirror. *Applied Optics*, 58(20):5366-5374. https://doi.org/10.1364/AO.58.005366

Ren JW, Chen XW, Wang B, et al., 2023. Design and Optimization of Dual-focal Vehicle Head-up Display Optical System Based on Single-optical Machine. *Acta Photonica Sinica*, 52(8):249-258. https://doi.org/10.3788/gzxb-20235208.082-2001

Ran SW, Liu XM, Lei XH, et al., 2022. Three-Dimensional Shape Measurement of Head-Up Display Virtual Image Based on Binocular Vision. *Acta Optica Sinica*, 42(19): 58-65. https://doi.org/10.3788/AOS202242.1912001

Sun YH, Wu SJ, Wang B, et al., 2024. Design and Optimization of a Parallax Display System with Variable Projection Distance. *Acta Optica Sinica*, 44(8):190-206. https://doi.org/10.3788/AOS-231914

Tian LM, Xue CX, 2024. Design of Variable Focal Plane Dual Projection Head-up Display System. *Acta Optica Sinica*, https://link.cnki.net/urlid/31.1252.O4.20240412.1638.1038

Wu P, Chen LF, Wei YT, et al., 2024. Research on Calibration and Detection of Optical Parameters for AR-HUD. *SAIC Motor*, 3:35-38. https://doi.org/10.3969/j.issn.1007-4554.2024.03.06

Wang T, Li HF, 2024. Dynamic Distortion Assessment in Automobile HeadUp Displays with Subjective Methods. *Acta Optica Sinica*, 44(05):296-305. https://doi.org/10.3788/AOS231831

Wang SL, Lin ZJ, Xu SX, et al., 2023. Research Progress of Vergence-Accommodation Conflict in Near-Eye Display Based on Augmented Reality. *Acta Optica Sinica*, 43(23):9-27. https://doi.org/10.3788/AOS231074

Xu N, Yu FZ, Xu J, et al., 2023. HUDNet: A dynamic calibration method for automotive augmented reality head-up-displays. *Displays*, 78:102453. https://doi.org/10.1016/j.displa.2023.102453

Yanusik I, Kalinina A, Morozov A, et al., 2021. Pupil replication waveguide system for autostereoscopic imaging with a wide field of view. *Optics Express*, 29(22):36287-36301. https://doi.org/10.1364/OE.439855

Yu ML, Li CH, Wu JC, et al., 2023. Exploring the Attention Level of AR-HUD Interface Elements Based on Driving Scenarios. 2023 14th International Conference on Mechanical and Intelligent Manufacturing Technologies (ICMIMT), p.117-121. https://doi.org/10.1109/ICMIMT59138.2023.10199531

Zhang YL, Su ZP, Pan HX, et al., 2020. Optical Design and Tolerance Analysis of Freeform Automotive Head-up Display. *Acta Photonica Sinica*, 49(9):1-12. https://doi.org/10.3788/gzxb2-0204909.0922002

Electronic supplementary materials

Eqs. (S1)–(S4)